On Fiber Dispersion Models: Exclusion of Compressed Fibers and Spurious Model Comparisons

Gerhard A. Holzapfel[1,2*] and Ray W. Ogden[3]

[1]Institute of Biomechanics, Graz University of Technology
Stremayrgasse 16-II, 8010 Graz, Austria

[2]Norwegian University of Science and Technology (NTNU)
Faculty of Engineering Science and Technology, 7491 Trondheim, Norway

[3]School of Mathematics and Statistics, University of Glasgow
University Gardens, Glasgow G12 8QW, Scotland, UK

To appear in the *Journal of Elasticity*
October 9, 2016

Abstract. Fiber dispersion in collagenous soft tissues has an important influence on the mechanical response, and the modeling of the collagen fiber architecture and its mechanics has developed significantly over the last few years. The purpose of the paper is twofold, first to develop a method for excluding compressed fibers within a dispersion for the generalized structure tensor (GST) model, which several times in the literature has been claimed not to be possible, and second to draw attention to several erroneous and misleading statements in the literature concerning the relative values of the GST and the angular integration (AI) model. For the GST model we develop a rather simple method involving a deformation dependent dispersion parameter that allows the mechanical influence of compressed fibers within a dispersion to be excluded. The theory is illustrated by application to simple extension and simple shear in order to highlight the effect of exclusion. By means of two examples we also show that the GST and the AI models have equivalent predictive power, contrary to some claims in the literature. We conclude that from the theoretical point of view neither of these two models is superior to the other. However, as is well known and as we now emphasize, the GST model has proved to be very successful in modeling the data from experiments on a wide range of tissues, and it is easier to analyze and simpler to implement than the AI approach, and the related computational effort is much lower.

Keywords: Fiber dispersion model; generalized structure tensor; angular integration model; fibrous tissue; exclusion of compressed fibers

*To whom correspondence should be addressed. Email address: holzapfel@tugraz.at

1 Introduction

Collagen fiber dispersion in fibrous tissues has been recognized as being important in the mechanical response of the tissue. In recent years continuum mechanical models of this response for tissues such as arteries, the myocardium, heart valves, corneas and articular cartilage have been developed to accommodate the effect of collagen fiber dispersion embedded within a non-collagenous matrix material. There are now many imaging modalities available that can identify fiber orientations within tissues; in particular, second-harmonic generation, see, e.g., [1], and ultra-high field diffusion tensor magnetic resonance imaging, see, e.g., [2]. These modalities are able to capture the 3D distribution of collagen fiber orientations without damage to the tissue, in contrast to histological investigations. This allows a detailed geometrical reconstruction of the fiber architecture which then serves as a basis for more advanced modeling including finite element analysis. It is often considered that in the modeling of such dispersions only those fibers which are extended should contribute to the mechanical response. In other words compression is supported only by the non-collagenous matrix material in which the fibers are embedded, and this consideration forms part of the motivation of the present work.

Basically there exist two different approaches for modeling fiber dispersion. First, the 'angular integration' (AI) approach, which is due to Lanir [3]. In this approach a single collagen fiber with strain energy $w(\lambda)$ is considered as a function of the fiber stretch λ. The strain energy is then integrated over a unit sphere Ω to obtain the strain-energy function Ψ of the aggregate of the fibers per unit reference volume, i.e.

$$\Psi = n \int_{\Omega} \rho(\mathbf{N}) w(\lambda) \mathrm{d}\Omega, \tag{1}$$

where $\mathbf{N}$ is a unit vector pointing in the direction of an arbitrary fiber, n is the number of fibers per unit reference volume, and ρ is the relative angular density of fibers normalized according to

$$\frac{1}{4\pi} \int_{\Omega} \rho(\mathbf{N}) \mathrm{d}\Omega = 1. \tag{2}$$

In (1) it has been assumed that the elastic properties of all the fibers are characterized by the same strain energy w, which was not the case in the original approach by Lanir [3].

Second, the 'generalized structure tensor' (GST) approach [4] considers an energy function Ψ_{f} associated with the fibers given by

$$\Psi_{\mathrm{f}} = \Psi_{\mathrm{f}}(\mathbf{C}, \mathbf{H}), \tag{3}$$

which involves the right Cauchy–Green tensor $\mathbf{C}$, and a generalized structure tensor $\mathbf{H}$, defined

by

$$\mathbf{H} = \frac{1}{4\pi} \int_{\Omega} \rho(\mathbf{N}) \mathbf{N} \otimes \mathbf{N} \mathrm{d}\Omega, \tag{4}$$

with the condition $\mathrm{tr}\mathbf{H} = 1$ following from the normalization (2). A list of relevant contributions to these two modeling approaches is provided in the introduction of [5].

Unfortunately, several errors concerning the relationships between the GST and the AI models have been promulgated in the literature, as in, e.g., [6], repeated in [7], [8], [9] and other studies. We therefore highlight some of the errors in order to discourage further repetitions.

First, according to [6], the GST model '*. . . gives excellent results for two reasons: (i) the fiber directional dispersion is small and (ii) all fibers are loaded in tension*'. Both these conclusions are false. The conclusion (i) is false because the argument is based on the very specialized assumption that the strain-energy function Ψ_{f} in (3) is the same as the strain-energy function w of an individual fiber, and the argument in [6] is also based on a Taylor expansion approximation of w around the mean fiber direction, which is itself only valid for small dispersions. The conclusion (ii) is false because in the application to arteries considered in [4] not all the fibers within the dispersion are loaded in tension but still the results are excellent. Indeed, because of incompressibility, at least one stretch always has to be less than one so that some fibers in a dispersion are always under compression. One implication of conclusion (ii) is that the GST model cannot exclude fibers in compression, which is certainly not the case. Indeed a simple procedure for excluding fibers in compression in the GST approach forms the first part of the content of the present paper. This also complements our analysis of the exclusion procedure in the AI approach contained in [10] and its implementation described in [11]. It should also be mentioned that recently an approach to exclusion of fibers in the GST model based on the use of a Heaviside function was developed in [12].

Second, there was also the suggestion in [13], on the basis of the analysis in [6], that the GST model, in particular the model in [4], is a '*. . . first order approximation*' of the AI model, again a false conclusion. Third, the errors in [6] have been propagated in subsequent papers without question. For example, in [7], with reference to [6], it is stated that '*. . . structure tensors can only be used when all the fibers are in tension and the angular distribution is small*'.

Fourth, in [7] further errors have been produced because the authors used the same set of parameters in the exponential forms of the strain-energy function in the AI and the GST approaches (this is a particular example of the assumption used in [6]), which leads to incorrect conclusions concerning the relative predictions of the two models. To elaborate on this point,

in the AI model the authors of [7] used the exponential form

$$w(\lambda) = \frac{c_1}{2c_2}\{\exp[c_2(\lambda^2 - 1)^2] - 1\}, \tag{5}$$

and for the GST model, for comparison, they used the strain-energy function

$$\Psi_{\rm f}(I_1, I_4) = \frac{k_1}{2k_2}\{\exp[k_2(\kappa I_1 + (1 - 3\kappa)I_4)^2] - 1\}, \tag{6}$$

where c_1, c_2, k_1, k_2 are material constants, while I_1 and I_4 are standard invariants and κ is the dispersion parameter. The use of (5) in the integration (1) is legitimate. However, in [7] the predictions of the models were compared by setting $k_1 = c_1$ and $k_2 = c_2$, which is a very restrictive assumption, and leads to erroneous comparisons, a point on which we will elaborate in Sect. 3.

The errors from both studies [6] and [7] have been accepted and further developed with additional errors in [8], and subsequent papers. However, the basis of the comparisons therein is invalid since in each case the same material parameters have been used for two different models. An example of an unfounded statement which is contained in [8] is: *'Numerical tests show that for all the loading cases for which GST models introduce large errors, such as uniaxial loading, shear and biaxial loading, the proposed model has a better performance, in the sense that it provides results closer to the ones furnished by an exact angle integration of the fiber orientation distribution'*. This statement is based on the incorrect comparison in [7]. The GST model does not introduce large errors.

The main justification for selecting a particular model is that it captures very well the underlying structure and physics and the data from experiments. It has to be emphasized that the GST approach has proved to be very successful in modeling the data from experiments on a wide range of tissues, including arteries, the myocardium, heart valves, corneas, and articular cartilage, while comparisons of the AI model with experimental data have been conducted to a much lesser extent. The basis of the comparative study in [7], which suggests that the AI model is superior to the GST model, is unfounded. There is no justification for such a conclusion on the basis of the analysis in [7] or for referring to the AI approach as the 'gold standard'. The purpose of the second part of the present paper is to demonstrate by an appropriate choice of parameters that the AI and the GST modeling approaches are equivalent in regard to their predictive capabilities. Nevertheless, it should be emphasized that the GST approach is more amenable to theoretical analysis than the AI approach. It is also simpler to implement and the related computational effort is much lower because it does not involve integrations.

The outline of the paper is as follows. In Sect. 2 we provide a summary of the equations governing the GST model with rotational symmetry and show how a simple (deformation de-

pendent) modification of the dispersion parameter is used to exclude compressed fibers in a dispersion. The resulting model, based on a generalized structure tensor, is then used to illustrate the consequences of the exclusion of compressed fibers in simple tension and in simple shear. It is shown, in particular, that for simple tension in the mean fiber direction the stress response with the fibers excluded is much stiffer than when they are not excluded when there is significant dispersion. On the other hand, depending on the mean fiber orientation, the simple shear stress response is either stiffer or softer with fiber exclusion than without the exclusion, again when there is significant dispersion.

In order to quantify our comments in the foregoing discussion relating to the studies in, e.g., [6], [7], [8], we provide in Sect. 3 an analysis of the comparison between the GST and AI models for small strains. In particular it is shown that the choice $k_1 = c_1$ and $k_2 = c_2$ in the equations (5) and (6), as in [7], is only valid in the two limiting cases of no dispersion or isotropic dispersion. In fact, to properly compare the predictions of the two models on the basis of the exponential models (5) and (6) the parameters c_1 and c_2 must depend not only on k_1 and k_2 but also on the dispersion parameter κ. We then go on to compare the predictions of the AI and the GST models for simple tension and simple shear for three different values of dispersion and in each case, with an appropriate choice of parameters, it can be seen that the predictions of the two models essentially coincide. This is in sharp contrast to the results in [7] for the same deformations.

2 GST model with excluded compressed fibers

We consider a deformation described in terms of the deformation gradient $\mathbf{F}$. The associated left and right Cauchy–Green tensors are $\mathbf{B} = \mathbf{F}\mathbf{F}^{\mathrm{T}}$ and $\mathbf{C} = \mathbf{F}^{\mathrm{T}}\mathbf{F}$, respectively. In Fig. 1 the unit vector $\mathbf{M}$ represents the mean fiber direction in the reference configuration of a fiber dispersion with an arbitrary fiber direction denoted $\mathbf{N}$, together with the cone within which the fibers are stretched in the deformed configuration, i.e. for which $(\mathbf{C}\mathbf{N})\cdot\mathbf{N} > 1$. Note that $\mathbf{M}$ is included in the cone but if $\mathbf{M}$ is compressed rather than extended then $\mathbf{C}\mathbf{N}\cdot\mathbf{N} > 1$ holds in the complement of the cone.

With respect to an orthonormal basis $\mathbf{E}_1$, $\mathbf{E}_2$, $\mathbf{E}_3$ with $\mathbf{M} = \mathbf{E}_3$, the unit vector $\mathbf{N}$ is given by

$$\mathbf{N} = \sin\Theta\cos\Phi\,\mathbf{E}_1 + \sin\Theta\sin\Phi\,\mathbf{E}_2 + \cos\Theta\,\mathbf{E}_3, \tag{7}$$

where $\Theta \in [0,\pi]$ and $\Phi \in [0,2\pi]$ are spherical polar angles, and $\mathbf{M}\cdot\mathbf{N} = \cos\Theta$. Then the equation $(\mathbf{C}\mathbf{N})\cdot\mathbf{N} = 1$ describes the boundary of the region in Fig. 1, and, with (7), the explicit

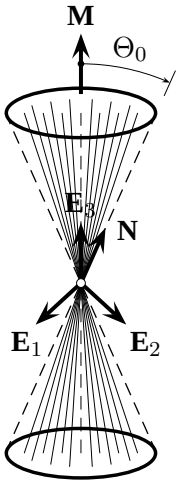

Figure 1: Unit vector **N** which defines the direction of an arbitrary fiber within a fiber dispersion, mean fiber direction **M** in the reference configuration and cone of fibers which are stretched in the deformed configuration, i.e. $(\mathbf{CN}) \cdot \mathbf{N} > 1$. An orthonormal basis $\mathbf{E}_1$, $\mathbf{E}_2$, $\mathbf{E}_3$ with $\mathbf{M} = \mathbf{E}_3$. Note that in general the cone is not symmetric about **M**, and in this example **M** satisfies $(\mathbf{CM}) \cdot \mathbf{M} > 1$.

expression reads

$$\begin{aligned}(\mathbf{CN}) \cdot \mathbf{N} = \sin^2\Theta(C_{11}\cos^2\Phi + 2C_{12}\sin\Phi\cos\Phi + C_{22}\sin^2\Phi) \\ +2\sin\Theta\cos\Theta(C_{13}\cos\Phi + C_{23}\sin\Phi) + C_{33}\cos^2\Theta = 1,\end{aligned} \tag{8}$$

which, of course, is satisfied identically in the reference configuration, C_{ij} being the components of **C**. When $\Theta \neq \pi/2$ Eq. (8) may be rearranged as

$$\begin{aligned}&\tan^2\Theta(C_{11}\cos^2\Phi + 2C_{12}\sin\Phi\cos\Phi + C_{22}\sin^2\Phi - 1) \\ &+2\tan\Theta(C_{13}\cos\Phi + C_{23}\sin\Phi) + C_{33} - 1 = 0,\end{aligned} \tag{9}$$

which is a quadratic in $\tan\Theta$ and shows that Θ depends on Φ and **C**. If $\Theta = \pi/2$ Eq. (8) reduces to

$$C_{11}\cos^2\Phi + 2C_{12}\sin\Phi\cos\Phi + C_{22}\sin^2\Phi = 1, \tag{10}$$

which governs unstretched fibers perpendicular to **M**.

Under the deformation, the mean fiber direction **M** maps into **FM** in the deformed configuration, and we use the notation $\mathbf{m} = \mathbf{FM}$ to represent this. In general, **m** is neither a unit vector nor the mean fiber direction in the deformed configuration. Correspondingly, for an arbitrary fiber we adopt the notation **n** defined by $\mathbf{n} = \mathbf{FN}$. Next we introduce the angle θ in the current

configuration, which, for a given **C**, is related to Θ and Φ by

$$\cos\theta = \frac{\mathbf{m}\cdot\mathbf{n}}{|\mathbf{m}||\mathbf{n}|} = \frac{(C_{13}\cos\Phi + C_{23}\sin\Phi)\sin\Theta + C_{33}\cos\Theta}{C_{33}^{1/2}|\mathbf{n}|} \tag{11}$$

since $|\mathbf{m}| = C_{33}^{1/2}$. The GST model uses a generalized structure tensor, as defined in Eq. (4). For the case in which the dispersion is rotationally symmetric about a mean direction **M**, following [4], the generalized structure tensor has the form $\mathbf{H} = \kappa\mathbf{I} + (1-3\kappa)\mathbf{M}\otimes\mathbf{M}$, and the (constant) dispersion parameter is defined by [4]

$$\kappa = \frac{1}{4}\int_0^\pi \rho(\Theta)\sin^3\Theta \mathrm{d}\Theta, \tag{12}$$

where $\rho(\Theta)$ is the fiber orientation density, rotationally symmetric about the mean fiber direction. It satisfies the normalization condition

$$\frac{1}{2}\int_0^\pi \rho(\Theta)\sin\Theta \mathrm{d}\Theta = 1 \tag{13}$$

and enjoys the symmetry properties

$$\rho(\pi+\Theta) = \rho(\pi-\Theta) = \rho(\Theta). \tag{14}$$

A generalized invariant denoted $I_4^\star$ associated with **H** is

$$I_4^\star = \mathrm{tr}(\mathbf{HC}) = \kappa I_1 + (1-3\kappa)I_4, \tag{15}$$

where

$$I_1 = \mathrm{tr}\mathbf{C}, \quad I_4 = \mathbf{M}\cdot(\mathbf{CM}). \tag{16}$$

We emphasize that (12) includes *all* the fibers in the dispersion whether they are in tension or compression. If we wish to exclude compressed fibers then an appropriate range of angles needs to be omitted from the integral in (12). Towards this goal we define a modified dispersion parameter, denoted $\kappa_1(\Theta)$, by

$$\kappa_1(\Theta) = \frac{1}{4}\int_0^\Theta \rho(\xi)\sin^3\xi \mathrm{d}\xi + \frac{1}{4}\int_{\pi-\Theta}^\pi \rho(\xi)\sin^3\xi \mathrm{d}\xi, \tag{17}$$

where $\Theta \in [0, \pi/2]$. The combination of integrals in (17) is appropriate for the case in which the mean fiber direction is extended, i.e. $(\mathbf{CM})\cdot\mathbf{M} > 1$. However, because of the symmetry properties (14) the two integrals are the same and hence (17) simplifies to

$$\kappa_1(\Theta) = \frac{1}{2}\int_0^\Theta \rho(\xi)\sin^3\xi \mathrm{d}\xi. \tag{18}$$

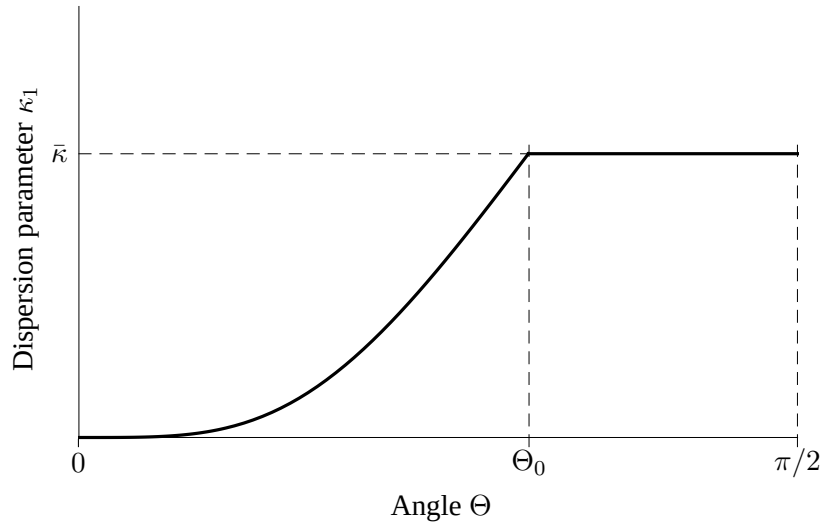

Figure 2: Typical plot of κ_1 vs Θ contained in $[0, \pi/2]$. For $0 \leq \Theta \leq \Theta_0$ the curve is determined by (18), while for $\Theta_0 \leq \Theta \leq \pi/2$, $\kappa_1(\Theta) = \kappa_1(\Theta_0)$, which we denote by $\bar{\kappa}$.

In particular, if $\Theta = \Theta_0$, which corresponds to the boundary of the cone shown in Fig. 1, then by (9) with Θ replaced by Θ_0 it is clear that Θ_0 depends on Φ and **C**. Then $\kappa_1(\Theta_0)$ is the dispersion parameter appropriate for the case in which the compressed fibers are excluded, and in this case $\kappa_1(\Theta_0)$ can be obtained from (12) by setting $\rho(\Theta) = 0$ for $\Theta_0 \leq \Theta \leq \pi - \Theta_0$. To illustrate its behavior a typical plot of $\kappa_1(\Theta)$ is shown in Fig. 2 for Θ between 0 and $\pi/2$. This shows that $\kappa_1(\Theta)$ increases monotonically from 0 to Θ_0 and has the value $\kappa_1(\Theta_0)$ for Θ between Θ_0 and $\pi/2$. From (18) it follows that

$$\kappa_1'(\Theta) = \frac{1}{2}\rho(\Theta)\sin^3\Theta \tag{19}$$

at any point where ρ is continuous but since we have set $\rho(\Theta_0) = 0$, κ_1' is discontinuous at $\Theta = \Theta_0$, with $\kappa_1'(\Theta) = 0$ for $\Theta_0^+ \leq \Theta \leq \pi/2$.

For convenience we now denote $\kappa_1(\Theta_0)$ by $\bar{\kappa}$ and consider the material to be incompressible with an energy function $\Psi(I_1, I_4, \bar{\kappa})$. Since $\kappa_1'(\Theta_0^+) = 0$ it follows that $\bar{\kappa}$ is stationary with respect to **C**, and hence the second Piola–Kirchhoff stress tensor **S** is given by

$$\mathbf{S} = 2\frac{\partial \Psi}{\partial \mathbf{C}} = 2\psi_1\mathbf{I} + 2\psi_4\mathbf{M}\otimes\mathbf{M} - p\mathbf{C}^{-1}, \tag{20}$$

where the abbreviations $\psi_1 = \partial\Psi/\partial I_1$ and $\psi_4 = \partial\Psi/\partial I_4$ have been used, and p is the Lagrange multiplier associated with the constraint $\det \mathbf{C} = 1$. Thus, while its derivative with respect to **C** does not appear in (20), $\bar{\kappa} = \kappa_1(\Theta_0)$ does depend on **C** and is incorporated in the expression for **S** in exactly the same way as if it were a constant. For example, with a typical energy function of the form

$$\Psi = \Psi_{\rm iso}(I_1) + \Psi_{\rm f}(I_4^\star), \tag{21}$$

we obtain the stress relation

$$\mathbf{S} = 2\Psi'_{\rm iso}(I_1)\mathbf{I} + 2\Psi'_{\rm f}(I_4^\star)\mathbf{H} - p\mathbf{C}^{-1}, \tag{22}$$

where $\Psi_{\rm iso}(I_1)$ represents the isotropic contribution related to the non-collagenous matrix material and $\Psi_{\rm f}(I_4^\star)$ is the contribution of the energy stored in the collagen fibers. In addition, $I_4^\star$ is now given by $I_4^\star = \bar{\kappa}I_1 + (1-3\bar{\kappa})I_4$, which is Eq. (15)$_2$ with κ replaced by $\bar{\kappa}$, and we emphasize that $\mathbf{H} = \bar{\kappa}\mathbf{I} + (1-3\bar{\kappa})\mathbf{M}\otimes\mathbf{M}$ now involves $\bar{\kappa}$ rather than κ.

If we consider the model adopted in [4] then, for a single family of fibers, we have

$$\Psi_{\rm iso}(I_1) = \frac{\mu}{2}(I_1 - 3), \quad \Psi_{\rm f}(I_4^\star) = \frac{k_1}{2k_2}\left\{\exp\left[k_2(I_4^\star - 1)^2\right] - 1\right\}, \tag{23}$$

where μ and k_1 are parameters with dimensions of stress and k_2 is a dimensionless parameter. Hence, from (22), the second Piola–Kirchhoff stress tensor becomes

$$\mathbf{S} = \mu\mathbf{I} + 2k_1(I_4^\star - 1)\exp\left[k_2(I_4^\star - 1)^2\right]\mathbf{H} - p\mathbf{C}^{-1}. \tag{24}$$

Similarly, if the mean fiber direction is not extended $(\mathbf{CM})\cdot\mathbf{M} \leq 1$ then $(\mathbf{CN})\cdot\mathbf{N} > 1$ for $\Theta \in (\Theta_0, \pi - \Theta_0)$, and in this case we define

$$\kappa_2(\Theta_0) = \frac{1}{4}\int\limits_{\Theta_0}^{\pi-\Theta_0} \rho(\Theta)\sin^3\Theta {\rm d}\Theta, \tag{25}$$

which is complementary to $\kappa_1(\Theta_0)$ and can be obtained from (12) by setting $\rho(\Theta) = 0$ for $\Theta \in [0, \Theta_0] \cup [\pi - \Theta_0, \pi]$. Note that

$$\kappa_1(\Theta_0) + \kappa_2(\Theta_0) = \kappa. \tag{26}$$

2.1 Example: Simple Tension

As a first example we consider a uniaxial stretch $\lambda \geq 1$ in the direction $\mathbf{M} = \mathbf{E}_3$ with a dispersion that is rotationally symmetric about $\mathbf{M}$. Then, by symmetry, the lateral stretches $\lambda_2 = \lambda_3$ are $\lambda^{-1/2}$, and the components of $\mathbf{F}$ are diag$[\lambda, \lambda^{-1/2}, \lambda^{-1/2}]$, so that Eq. (11) reduces to

$$\cos\theta = \frac{\lambda\cos\Theta}{\sqrt{\lambda^2\cos^2\Theta + \lambda^{-1}\sin^2\Theta}}. \tag{27}$$

Note, in particular, that on the boundary of the cone Eq. (8) reduces to

$$I_4 = \lambda^2\cos^2\Theta + \lambda^{-1}\sin^2\Theta = 1, \tag{28}$$

which, for $\lambda \neq 1$, can be rearranged with $\Theta = \Theta_0$ as

$$\tan \Theta_0 = \sqrt{\lambda(\lambda+1)}. \tag{29}$$

It follows that $\cos\theta_0 = \lambda \cos\Theta_0$, where θ_0 is the value θ obtained from (27) when (28) holds. If $0 \leq \Theta < \Theta_0$ and $\pi - \Theta_0 < \Theta \leq \pi$ then the fibers are extended. Thus, as λ increases more and more fibers are recruited into extension, and Θ_0 becomes larger and approaches $\pi/2$, while θ_0 tends to zero.

We now consider the energy function $\Psi^\star(I_1, I_4^\star) = \Psi(I_1, I_4, \bar{\kappa})$ with $\bar{\kappa} = \kappa_1(\Theta_0)$. Then the Cauchy stress tensor $\boldsymbol{\sigma} = \mathbf{FSF}^{\mathrm{T}}$ is given by

$$\boldsymbol{\sigma} = 2\psi_1^\star \mathbf{B} + 2\psi_4^\star \mathbf{h} - p\mathbf{I}, \tag{30}$$

where $\psi_1^\star = \partial\Psi^\star/\partial I_1$ and $\psi_4^\star = \partial\Psi^\star/\partial I_4^\star$ and

$$\mathbf{h} = \bar{\kappa}\mathbf{B} + (1-3\bar{\kappa})\mathbf{m}\otimes\mathbf{m}, \quad I_4^\star = \bar{\kappa}I_1 + (1-3\bar{\kappa})I_4 = \lambda^2 - 2\bar{\kappa}(\lambda^2 - \lambda^{-1}), \tag{31}$$

$\mathbf{h} = \mathbf{FHF}^{\mathrm{T}}$ being the spatial generalized structure tensor. For the model (23) we have

$$\psi_1^\star = \mu/2, \quad \psi_4^\star = k_1(I_4^\star - 1)\exp[k_2(I_4^\star - 1)^2]. \tag{32}$$

For simple tension let σ be the component of the Cauchy stress in the direction of stretch. Then, by specializing (30), we obtain

$$\sigma = \mu\lambda^2 + 2k_1(I_4^\star - 1)\exp[k_2(I_4^\star - 1)^2][\bar{\kappa}\lambda^2 + (1-3\bar{\kappa})\lambda^2] - p, \tag{33}$$

$$0 = \mu\lambda^{-1} + 2k_1(I_4^\star - 1)\exp[k_2(I_4^\star - 1)^2]\bar{\kappa}\lambda^{-1} - p, \tag{34}$$

and hence, on elimination of p,

$$\begin{aligned}\sigma = {} & \mu(\lambda^2 - \lambda^{-1}) + 2k_1[\lambda^2 - 1 - 2\bar{\kappa}(\lambda^2 - \lambda^{-1})](\lambda^2 - 2\bar{\kappa}\lambda^2 - \bar{\kappa}\lambda^{-1}) \\ & \times \exp\left\{k_2[\lambda^2 - 1 - 2\bar{\kappa}(\lambda^2 - \lambda^{-1})]^2\right\}.\end{aligned} \tag{35}$$

We emphasize here that $\bar{\kappa} = \kappa_1(\Theta_0)$ depends on λ via (29).

In order to compare the behavior of the model where compressed fibers are excluded with the model where they are not excluded, i.e. with a constant κ, we adopt the von Mises distribution used in [4]. This is given by

$$\rho(\Theta) = 4\sqrt{\frac{b}{2\pi}}\frac{\exp(2b\cos^2\Theta)}{\operatorname{erfi}(\sqrt{2b})}, \tag{36}$$

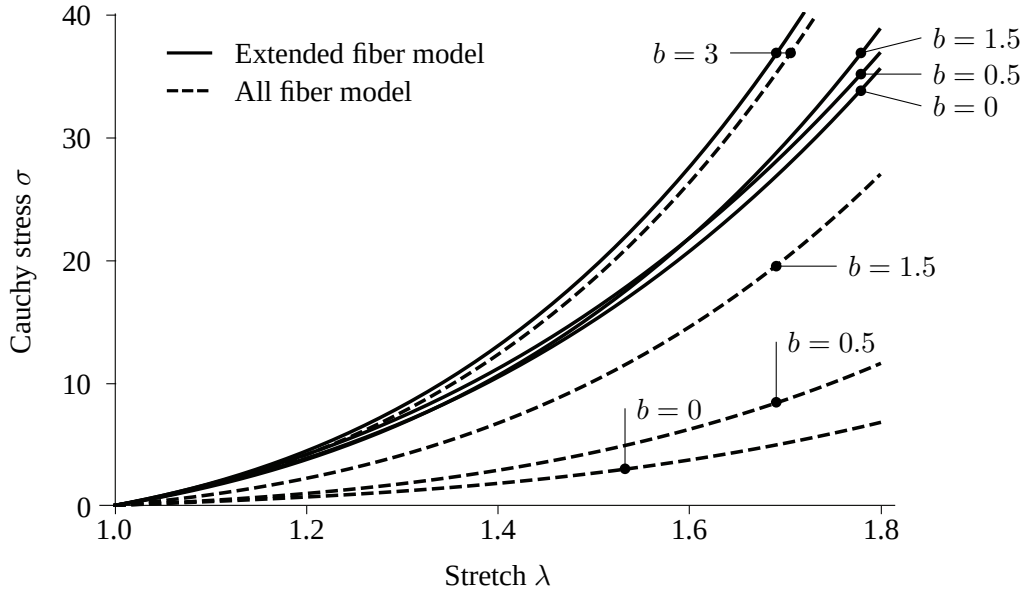

Figure 3: Uniaxial Cauchy stress σ against the corresponding stretch λ for the four values $b = 0, 0.5, 1.5, 3$ (corresponding to $\kappa = 1/3, 0.285, 0.187, 0.096$) and for $k_1/\mu = 5$ and $k_2 = 0.01$.

where erfi is the imaginary error function and b is the concentration parameter. In fact, a specific formula can be obtained for κ by using (36) in the definition (12) with the help of Mathematica [14]. This is

$$\kappa = \frac{1}{2} + \frac{1}{8b} - \frac{1}{4}\sqrt{\frac{2}{\pi b}}\frac{\exp(2b)}{\mathrm{erfi}(\sqrt{2b})}, \tag{37}$$

as given in [15], and it can also be obtained from the formula for the out-of-plane dispersion parameter κ_{op} given in equation (2.28) of [5] by replacing b by $-b$.

We now consider the energy function Ψ specified in (23) and use $k_1/\mu = 5$ and $k_2 = 0.01$, and the values of $b = 0, 0.5, 1.5, 3$ which correspond to $\kappa = 1/3, 0.285, 0.187, 0.096$, respectively. Figure 3 shows plots of the uniaxial Cauchy stress σ versus the corresponding stretch λ based on (35) for the four values of b. The solid curves refer to the model described here while the dashed curves correspond to the case with no fibers excluded and constant κ. As can be seen, as the value of b increases a smaller and smaller proportion of fibers are compressed and hence the difference between the two models decreases; most of the fibers are then aligned with the direction of tension, and the response is stiffest, and if $b \to \infty$, then the curves are identical. For smaller values of b and hence more dispersion there is a significant difference between the two models, and in each case the response is stiffest for the new model. This can be seen from the analytical expression (35) since $\bar{\kappa}$ is smaller than κ. As can be seen from Fig. 3 the continuous curve for $b = 0.5$ crosses over that for $b = 1.5$. This is because for $b = 0.5$, $\bar{\kappa}$

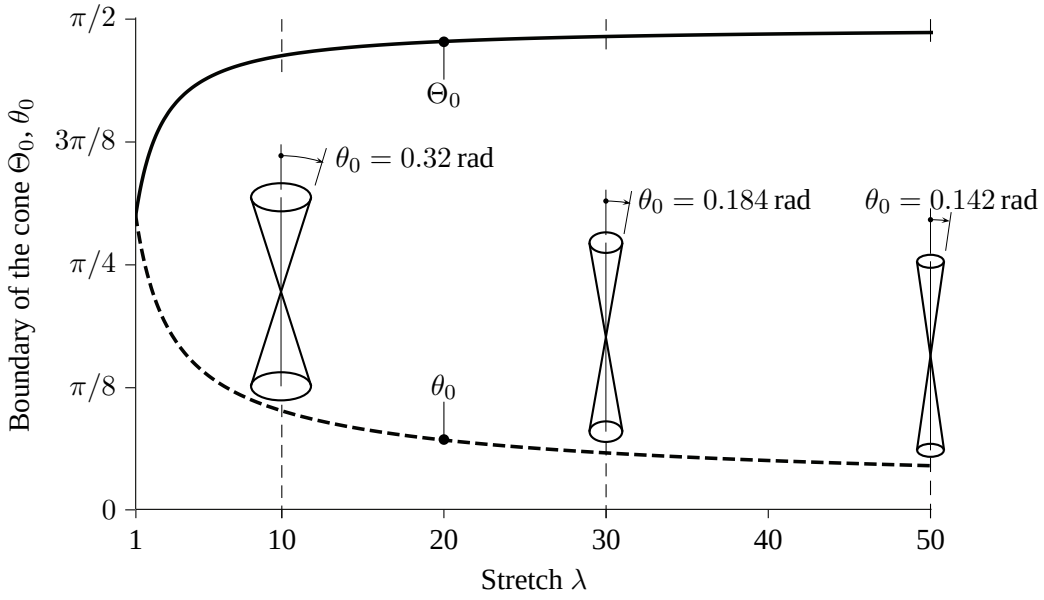

Figure 4: Evolution of Θ_0 and θ_0 with stretch λ. Cone $\theta_0 = 0.32, 0.184, 0.142$ rad of stretched fibers in the deformed configuration for three representative values $\lambda = 10, 30, 50$.

grows faster with λ initially than for $b = 1.5$.

Figure 4 shows the evolution of Θ_0 and θ_0 with stretch λ. As can be seen from the plots the cone of stretched fibers in the deformed configuration is shown for three representative values of λ $(10, 30, 50)$, and we note that the angle of the cone decreases as the value of λ increases (for $\lambda = 10, 30, 50$, $\theta_0 = 0.32, 0.184, 0.142$ rad, respectively). The corresponding cones for the fibers in the reference configuration which are stretched in the deformed configuration are not shown, but we record that the angles for these cones increase with λ (for $\lambda = 10, 30, 50$, $\Theta_0 = 1.476, 1.538, 1.551$ rad, respectively).

2.2 Example: Simple Shear in the $(1, 2)$-plane

For the second example we consider simple shear in the $\mathbf{E}_1$-direction in the $(\mathbf{E}_1, \mathbf{E}_2)$-plane, with dispersed fibers lying in this plane. The components of the deformation gradient and the right Cauchy–Green tensors are

$$[\mathbf{F}] = \begin{bmatrix} 1 & \gamma & 0 \\ 0 & 1 & 0 \\ 0 & 0 & 1 \end{bmatrix}, \quad [\mathbf{C}] = \begin{bmatrix} 1 & \gamma & 0 \\ \gamma & 1+\gamma^2 & 0 \\ 0 & 0 & 1 \end{bmatrix}, \tag{38}$$

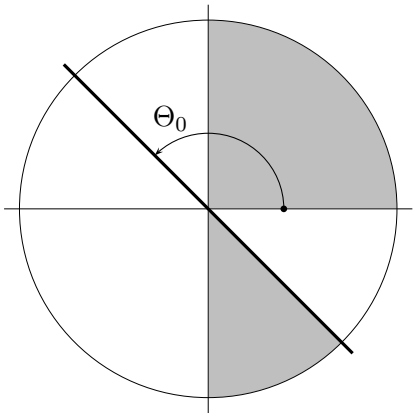

Figure 5: Depiction of the region in the $(1,2)$ space traced out by the unit vector **N** in (39) for $0 \leq \Theta \leq 2\pi$. Within the half-circle $-\pi/2 \leq \Theta \leq \pi/2$ the shaded regions $-\pi/2 \leq \Theta < -(\pi - \Theta_0)$ and $0 < \Theta \leq \pi/2$ are defined by $(\mathbf{CN}) \cdot \mathbf{N} > 1$. The angle Θ_0 satisfies (43) and ranges from $\pi/2$ for $\gamma = 0$ to π for $\gamma \to \infty$.

respectively, where $\gamma \geq 0$ is the amount of shear, and we take an arbitrary fiber direction **N** to have the form

$$\mathbf{N} = \cos\Theta \mathbf{E}_1 + \sin\Theta \mathbf{E}_2 \tag{39}$$

within a dispersion in the $(1,2)$-plane which has mean fiber direction **M** in that plane given by

$$\mathbf{M} = \cos\Theta_{\mathrm{M}} \mathbf{E}_1 + \sin\Theta_{\mathrm{M}} \mathbf{E}_2. \tag{40}$$

Then

$$(\mathbf{CN}) \cdot \mathbf{N} = 1 + \gamma \sin\Theta(\gamma \sin\Theta + 2\cos\Theta). \tag{41}$$

Since $\gamma \geq 0$, it follows that $(\mathbf{CN}) \cdot \mathbf{N} = 1$ for $\gamma = 0$ or $\Theta = 0$ and, provided $\Theta \neq 0$, $(\mathbf{CN}) \cdot \mathbf{N} > 1$ for

$$\sin\Theta(\gamma \sin\Theta + 2\cos\Theta) > 0. \tag{42}$$

Moreover, $(\mathbf{CN}) \cdot \mathbf{N} = 1$ for $\Theta = \Theta_0$ given by

$$\tan\Theta_0 = -\frac{2}{\gamma}. \tag{43}$$

If we restrict the attention to the range of values $\Theta \in [-\pi/2, \pi/2]$, then $(\mathbf{CN}) \cdot \mathbf{N} > 1$ for the shaded region in Fig. 5, i.e. for $-\pi/2 \leq \Theta < -(\pi - \Theta_0)$ and $0 < \Theta \leq \pi/2$. Equivalently, $(\mathbf{CN}) \cdot \mathbf{N} > 1$ for the range $0 < \Theta < \Theta_0$. Note that this is independent of whether the mean fiber direction **M** is compressed or extended.

Assuming the symmetry $\rho(\Theta+\pi) = \rho(\Theta)$ for the considered 2D dispersion with orientation distribution $\rho(\Theta)$, the normalization condition is

$$\frac{1}{\pi} \int_{-\pi/2}^{\pi/2} \rho(\Theta) \mathrm{d}\Theta = 1. \tag{44}$$

For this case the von Mises distribution $\rho(\Theta)$ symmetric about $\Theta = 0$ is given by

$$\rho(\Theta) = \frac{\exp(b \cos 2\Theta)}{I_0(b)}, \tag{45}$$

where I_0 is the modified Bessel function of the first kind of order 0. Without omitting any directions the dispersion parameter is defined by

$$\kappa = \frac{1}{\pi} \int_{-\pi/2}^{\pi/2} \rho(\Theta) \sin^2 \Theta \mathrm{d}\Theta = \frac{1}{2} \left(1 - \frac{I_1(b)}{I_0(b)} \right), \tag{46}$$

where $I_1(b)$ is the modified Bessel function of the first kind of order 1. The corresponding (generalized) structure tensor is

$$\hat{\mathbf{H}} = \kappa \hat{\mathbf{I}} + (1 - 2\kappa) \mathbf{M} \otimes \mathbf{M} \tag{47}$$

with $\mathbf{M} = \mathbf{E}_1$, where the hat indicates restriction in the $(1, 2)$ plane. For a general mean fiber direction $\mathbf{M}$, given in (40), the structure tensor again has the form (47).

Similarly to the three-dimensional case we define $\kappa_1(\Theta)$ according to

$$\kappa_1(\Theta) = \frac{1}{\pi} \int_{-\pi/2}^{-(\pi-\Theta)} \rho(\xi) \sin^2 \xi \mathrm{d}\xi + \frac{1}{\pi} \int_{0}^{\pi/2} \rho(\xi) \sin^2 \xi \mathrm{d}\xi. \tag{48}$$

Equivalently, because of the symmetry of ρ, this can be expressed as

$$\kappa_1(\Theta) = \frac{1}{\pi} \int_{0}^{\Theta} \rho(\xi) \sin^2 \xi \mathrm{d}\xi, \tag{49}$$

with $\Theta \in [0, \pi]$, and hence

$$\kappa_1'(\Theta) = \frac{1}{\pi} \rho(\Theta) \sin^2(\Theta). \tag{50}$$

Similarly to the three-dimensional case Eq. (49) can be obtained by setting $\rho(\Theta) = 0$ for $\Theta \in [\Theta_0, \pi]$, so $\rho(\Theta_0) = 0$ and hence $\kappa_1'(\Theta) = 0$ for $\Theta_0 \leq \Theta \leq \pi$.

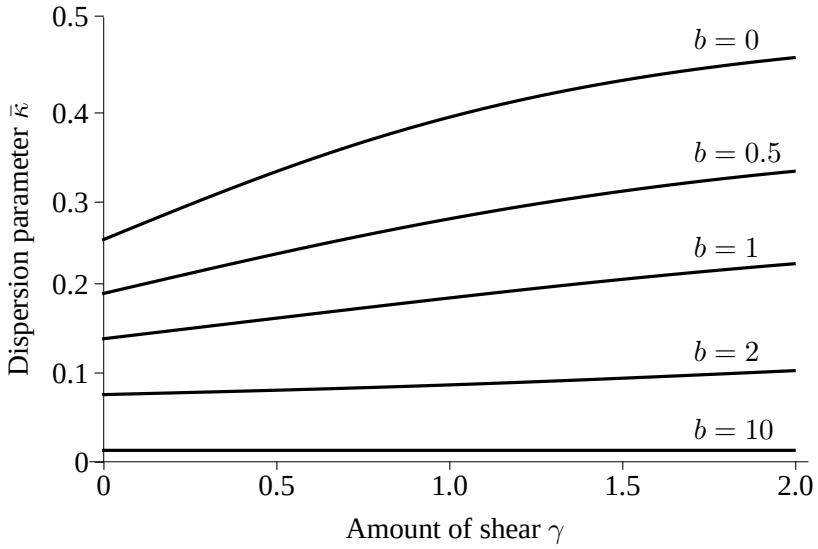

Figure 6: Example for simple shear showing the dependence of the dispersion parameter $\bar{\kappa} = \kappa_1(\Theta_0)$ on the amount of shear γ for different values of the concentration parameter b, when compressed fibers are excluded.

As in the three-dimensional case we use the notation $\bar{\kappa} = \kappa_1(\Theta_0)$. Representative plots of $\bar{\kappa} = \kappa_1(\Theta_0)$ as a function of γ for different values of the concentration parameter b are shown in Fig. 6 based on Eq. (49) with $\Theta = \Theta_0$ given by (43).

Consider again the model $\Psi^\star(I_1, I_4^\star)$ but now with the restriction to plane strain. Then, similarly to the three-dimensional case, the two-dimensional Cauchy stress is obtained as the specialization of (30), written as

$$\hat{\boldsymbol{\sigma}} = 2\psi_1^\star \hat{\mathbf{B}} + 2\psi_4^\star \hat{\mathbf{h}} - p\hat{\mathbf{I}}, \tag{51}$$

where a hat again signifies the restriction to two dimensions, so that $\hat{\mathbf{h}} = \bar{\kappa}\hat{\mathbf{B}} + (1 - 2\bar{\kappa})\mathbf{m} \otimes \mathbf{m}$. For simple shear we have

$$[\mathbf{m}] = [\mathbf{F}][\mathbf{M}] = \begin{bmatrix} M_1 + \gamma M_2 \\ M_2 \\ 0 \end{bmatrix}, \quad [\mathbf{B}] = \begin{bmatrix} 1 + \gamma^2 & \gamma & 0 \\ \gamma & 1 & 0 \\ 0 & 0 & 1 \end{bmatrix}, \tag{52}$$

where $[\mathbf{M}] = [M_1, M_2, 0] = [\cos\Theta_{\mathrm{M}}, \sin\Theta_{\mathrm{M}}, 0]$, and

$$\hat{I}_1 = \mathrm{tr}\hat{\mathbf{B}} = 2 + \gamma^2, \qquad \hat{I}_4^\star = \bar{\kappa}(2 + \gamma^2) + (1 - 2\bar{\kappa})(1 + 2\gamma M_1 M_2 + \gamma^2 M_2^2). \tag{53}$$

For the considered plane strain the strain-energy function (23) takes on the form

$$\Psi = \frac{\mu}{2}(\hat{I}_1 - 2) + \frac{k_1}{2k_2}\left\{\exp\left[k_2(\hat{I}_4^\star - 1)^2\right] - 1\right\}, \tag{54}$$

and the in-plane Cauchy stress components are derived as

$$\hat{\sigma}_{11} = \mu(1+\gamma^2) + 2\psi_4^\star[\bar{\kappa}(1+\gamma^2) + (1-2\bar{\kappa})(M_1+\gamma M_2)^2] - p, \tag{55}$$

$$\hat{\sigma}_{22} = \mu + 2\psi_4^\star[\bar{\kappa} + (1-2\bar{\kappa})M_2^2] - p, \tag{56}$$

$$\hat{\sigma}_{12} = \mu\gamma + 2\psi_4^\star[\bar{\kappa}\gamma + (1-2\bar{\kappa})(M_1+\gamma M_2)M_2]. \tag{57}$$

Of particular interest is the dependence of the shear stress $\hat{\sigma}_{12}$ on the amount of shear γ, and henceforth we focus on this relationship. First, however, we note that for a general direction (39) we have $\hat{I}_4 = 1 + \gamma \sin 2\Theta + \gamma^2 \sin^2\Theta$, which has its maximum value at $\Theta = \Theta_{\max}$ given by

$$\tan(2\Theta_{\max}) = -\frac{2}{\gamma}, \tag{58}$$

an equation which should be compared with (43). It follows that $\Theta_{\max} = \Theta_0/2$ and this ranges from $\pi/4$ at $\gamma = 0$ to $\pi/2$ as $\gamma \to \infty$. Thus, the direction in which the stretch is largest is close to $\Theta = \pi/4$ for moderate values of γ and this has a strong influence on the stiffness of the shear response. In particular, for the range $\gamma \in [0, 2]$ considered in the subsequent examples $\Theta_{\max} \in [\pi/4, 3\pi/8]$.

The following four illustrative examples are now considered.

Example 1: $\Theta_{\rm M} = 0$, $\hat{I}_4^\star - 1 = \bar{\kappa}\gamma^2$, with

$$\hat{\sigma}_{12} = \mu\gamma + 2k_1\bar{\kappa}^2\gamma^3 \exp(k_2\bar{\kappa}^2\gamma^4). \tag{59}$$

Example 2: $\Theta_{\rm M} = \pi/4$, $\hat{I}_4^\star - 1 = \gamma + \frac{1}{2}\gamma^2 - 2\bar{\kappa}\gamma$, with

$$\hat{\sigma}_{12} = \mu\gamma + k_1(I_4^\star - 1)\exp[k_2(I_4^\star - 1)^2](\gamma + 1 - 2\bar{\kappa}). \tag{60}$$

Example 3: $\Theta_{\rm M} = \pi/2$, $\hat{I}_4^\star - 1 = (1-\bar{\kappa})\gamma^2$, with

$$\hat{\sigma}_{12} = \mu\gamma + 2k_1(1-\bar{\kappa})^2\gamma^3 \exp[k_2(1-\bar{\kappa})^2\gamma^4]. \tag{61}$$

Example 4: $\Theta_{\rm M} = 3\pi/4$, $\hat{I}_4^\star - 1 = -\gamma + \frac{1}{2}\gamma^2 + 2\bar{\kappa}\gamma$, with

$$\hat{\sigma}_{12} = \mu\gamma + k_1(\hat{I}_4^\star - 1)\exp[k_2(\hat{I}_4^\star - 1)^2](\gamma - 1 + 2\bar{\kappa}). \tag{62}$$

We now compare the shear stress $\hat{\sigma}_{12}$ versus the amount of shear γ behavior for the model in which compressed fibers are omitted with that in which all fibers are included for these four representative examples. The results are shown in Fig. 7 for $b = 0.1, 1, 10$, which correspond to $\kappa = 0.475, 0.277, 0.026$, respectively. We choose $k_1/\mu = 5$ and $k_2 = 0.01$ and take these

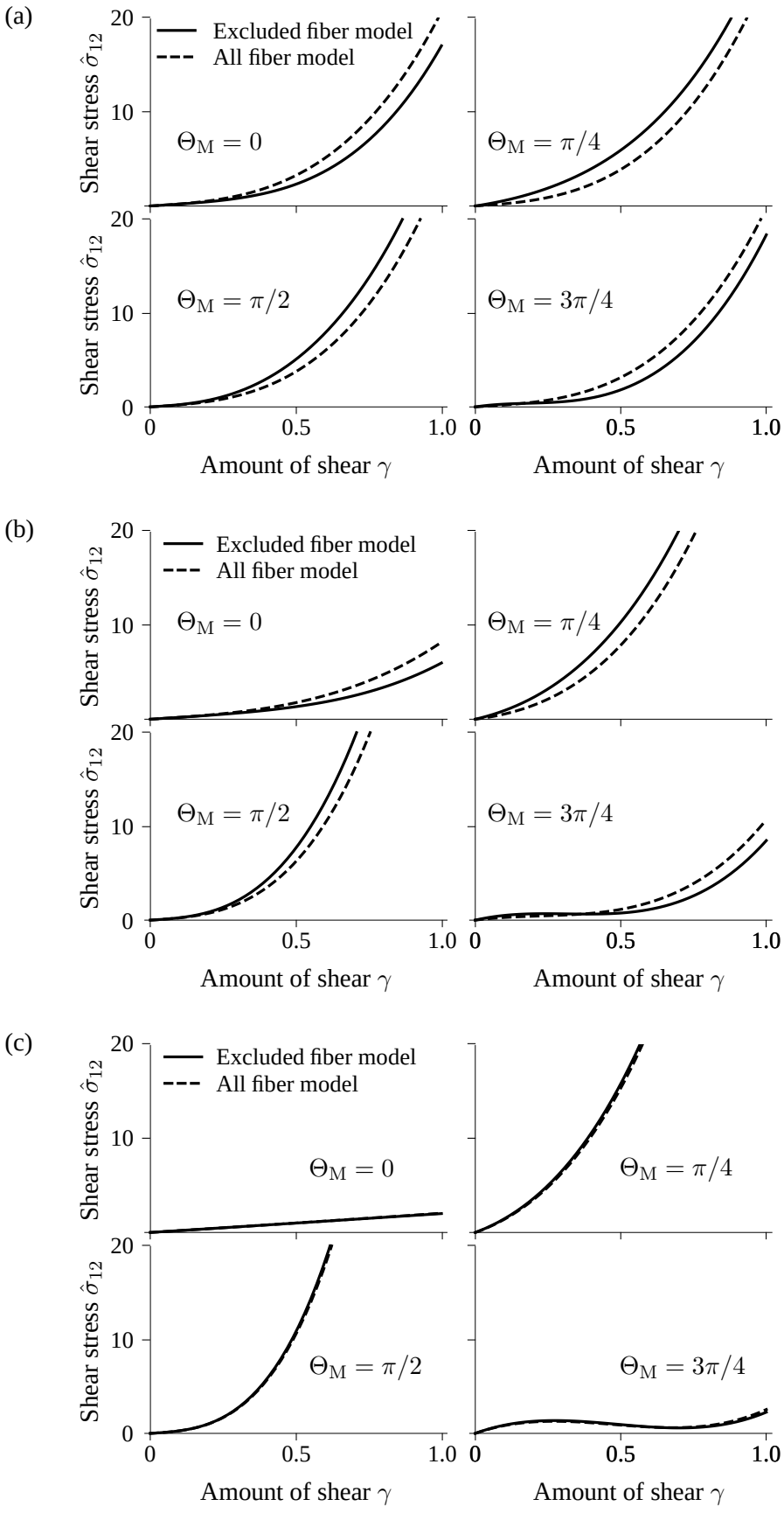

Figure 7: Shear stress $\hat{\sigma}_{12}$ versus amount of shear γ for both the excluded fiber model (continuous curves) and the 'all fiber' model (dashed curves) for $\Theta_{\mathrm{M}} = 0, \pi/4, \pi/2, 3\pi/4$: (a) $b = 0.1$ ($\kappa = 0.475$); (b) $b = 1$ ($\kappa = 0.277$); (c) $b = 10$ ($\kappa = 0.026$). For each case $k_1/\mu = 5$ and $k_2 = 0.01$.

values for purposes of illustration but the qualitative nature of the plots is very similar for other values.

First, for $b = 10$, we note that there is no essential difference between the plots with or without compressed fibers excluded (and the slight difference disappears altogether as b becomes larger and larger). This is because there is very little dispersion and the fibers are concentrated close to the mean fiber direction. For $\Theta_{\rm M} = 3\pi/4$, in particular, we note that the mean fiber direction is outside the range of integration for small values of γ so that the fibers do not contribute to the strain energy or stress initially, which is supported only by the isotropic term. As γ increases the fiber contribution to the stress is slightly negative for a small range of values of γ and leads to a maximum in the shear stress versus amount of shear behavior. Thereafter the fiber contribution becomes positive and increases rapidly with $\gamma > 2$ (not shown). Note that for $\Theta_{\rm M} = 0$ the stress is relatively small since for simple shear there is no stretch in the direction of shear. On the other hand, for $\Theta_{\rm M} = \pi/4$ and $\Theta_{\rm M} = \pi/2$, which are close to the direction of maximum stretch, the stress is much larger.

The pattern is similar for $b = 1$ in respect of the stress magnitudes although they are larger for $\Theta_{\rm M} = 0$ and $\Theta_{\rm M} = 3\pi/4$ because of the dispersion and there is a difference between the two models. For these two angles the 'all fiber' model has a higher stress than the excluded fiber model, but for $\Theta_{\rm M} = \pi/4$ and $\Theta_{\rm M} = \pi/2$ it is the other way around. And the situation for $b = 0.1$ is similar to that for $b = 1$ except that the stiffnesses for all four mean fiber directions are very similar, because this is very close to the isotropic situation. These differences can be seen in the Eqs. (59)–(62) since for Examples 1 and 4 the $\bar{\kappa}$ terms are positive, while in the Examples 2 and 3 they are negative. Thus, in contrast to uniaxial extension, for which the excluded fiber model gives a stiffer response than the all fiber model, in simple shear the stress can be either stiffer or softer depending on the mean fiber direction.

3 Some comparisons with the AI model

We now compare the GST model with the AI model due to Lanir [3] but without excluding compressed fibers. For the AI model the energy function is an integral of the form

$$n \int_{\Omega} \rho(\Theta, \Phi) w(\lambda) \sin\Theta \, \mathrm{d}\Theta \, \mathrm{d}\Phi, \tag{63}$$

where Ω is the unit sphere $\{(\Theta, \Phi) \,|\, \Theta \in [0, \pi],\ \Phi \in [0, 2\pi]\}$, the orientation density ρ depends on Θ and Φ in general, as does λ, which is defined as $\sqrt{I_4}$, where $I_4 = \mathbf{N} \cdot (\mathbf{CN})$, with $\mathbf{N}$ given by (7), for a general Cauchy–Green tensor $\mathbf{C}$, and $w(\lambda)$ is the strain energy of an individual

fiber in the direction **N**. Note that (63) does not include an isotropic term associated with the non-collagenous matrix material.

For purposes of comparison we include a neo-Hookean isotropic term and characterize the AI model by the strain-energy function $\Psi_{\rm AI}$ as

$$\Psi_{\rm AI} = \frac{1}{2}\mu(I_1 - 3) + n\int_\Omega \rho(\Theta,\Phi)w(\lambda)\sin\Theta\,{\rm d}\Theta\,{\rm d}\Phi. \tag{64}$$

The corresponding GST model has the form of (21) and (23), which we now write as

$$\Psi_{\rm GST} = \frac{1}{2}\mu(I_1 - 3) + \Psi_{\rm f}(I_4^\star), \tag{65}$$

where $\Psi_{\rm f}$ represents the strain energy of the dispersed fibers, and, for a rotationally symmetric dispersion, $I_4^\star$ is given by (15). Assuming that no energy or stress is associated with the fibers in the reference configuration, we have

$$w(1) = w'(1) = 0, \qquad \Psi_{\rm f}(1) = \Psi_{\rm f}'(1) = 0. \tag{66}$$

In the paper [7] it was attempted to compare the predictions of the above GST model with the AI model having the same exponential forms (5) and (6) and the same material constants $c_1 = k_1$ and $c_2 = k_2$. The associated Cauchy stress relations are

$$\boldsymbol{\sigma}_{\rm AI} = \mu\mathbf{B} + 2nc_1\int_\Omega \rho(\Theta,\Phi)(I_4 - 1)\exp[c_2(I_4 - 1)^2]\mathbf{n}\otimes\mathbf{n}\sin\Theta\,{\rm d}\Theta\,{\rm d}\Phi - p\mathbf{I} \tag{67}$$

and

$$\boldsymbol{\sigma}_{\rm GST} = \mu\mathbf{B} + 2k_1(I_4^\star - 1)\exp[k_2(I_4^\star - 1)^2][\kappa\mathbf{B} + (1 - 3\kappa)\mathbf{m}\otimes\mathbf{m}] - p\mathbf{I}, \tag{68}$$

where we recall that $\mathbf{n} = \mathbf{FN}$ and $\mathbf{m} = \mathbf{FM}$.

We now elaborate on this particular point by considering the case of small strains. The Green–Lagrange strain tensor $\mathbf{E}$ is defined by $\mathbf{E} = (\mathbf{C} - \mathbf{I})/2$, so that $I_1 = 3 + 2{\rm tr}\mathbf{E}$ and $I_4 = 1 + 2\mathbf{N}\cdot(\mathbf{EN})$. These expressions for the invariants are exact but when we expand $w(\lambda)$ and $\Psi_{\rm f}(I_4^\star)$ to the second order in $\mathbf{E}$ we obtain

$$w(\lambda) \approx \frac{1}{2}(\mathbf{N}\cdot\mathbf{EN})^2 w''(1), \qquad \Psi_{\rm f}(I_4^\star) \approx 2\Psi_{\rm f}''(1)(1 - 3\kappa)^2[\mathbf{M}\cdot(\mathbf{EM})]^2, \tag{69}$$

where the properties (66) have been used. By substituting these approximations into (64) and (65) we obtain

$$\Psi_{\rm AI} = \mu{\rm tr}\mathbf{E} + \frac{n}{2}w''(1)\int_\Omega \rho(\Theta,\Phi)[\mathbf{N}\cdot(\mathbf{EN})]^2\sin\Theta\,{\rm d}\Theta\,{\rm d}\Phi, \tag{70}$$

and

$$\Psi_{\rm GST} = \mu{\rm tr}\mathbf{E} + 2\Psi_{\rm f}''(1)(1 - 3\kappa)^2[\mathbf{M}\cdot(\mathbf{EM})]^2, \tag{71}$$

respectively. Note that, since we are considering incompressible materials, expansion of the incompressibility condition $\det \mathbf{C} = 1$ to the second order gives $\mathrm{tr}\mathbf{E} = \mathrm{tr}(\mathbf{E}^2)$, which can be used in (70) and (71). The corresponding linearized Cauchy stresses are deduced from (70) and (71) according to

$$\boldsymbol{\sigma}_{\mathrm{AI}} = 2\mu\mathbf{E} + nw''(1)\int_{\Omega}\rho(\Theta,\Phi)[\mathbf{N}\cdot(\mathbf{E}\mathbf{N})]\mathbf{N}\otimes\mathbf{N}\sin\Theta\,\mathrm{d}\Theta\,\mathrm{d}\Phi - p\mathbf{I} \tag{72}$$

and

$$\boldsymbol{\sigma}_{\mathrm{GST}} = 2\mu\mathbf{E} + 4\Psi_{\mathrm{f}}''(1)(1-3\kappa)^2[\mathbf{M}\cdot(\mathbf{E}\mathbf{M})]\mathbf{M}\otimes\mathbf{M} - p\mathbf{I}, \tag{73}$$

respectively.

For definiteness we now consider a uniaxial strain with component ε in the direction $\mathbf{M} = \mathbf{E}_3$, with Θ measured from $\mathbf{E}_3$ and with ρ independent of Φ. Then, the dispersion is rotationally symmetric about $\mathbf{E}_3$ and, by symmetry and the incompressibility condition, the lateral strains are, to the first order, each equal to $-\varepsilon/2$. By using the definition (7) and $\mathbf{M} = \mathbf{E}_3$ it follows that $\mathbf{M}\cdot(\mathbf{E}\mathbf{M}) = \varepsilon$ and $\mathbf{N}\cdot(\mathbf{E}\mathbf{N}) = (3\cos^2\Theta - 1)\varepsilon/2$. The corresponding uniaxial stresses after elimination of p are obtained as

$$\sigma_{\mathrm{AI}} = 3\mu\varepsilon + \frac{n\pi}{2}w''(1)f(b)\varepsilon, \qquad \sigma_{\mathrm{GST}} = 3\mu\varepsilon + 4\Psi_{\mathrm{f}}''(1)(1-3\kappa)^2\varepsilon, \tag{74}$$

where

$$f(b) = \int_0^{\pi}\rho(\Theta)(3\cos^2\Theta - 1)^2\sin\Theta\,\mathrm{d}\Theta, \tag{75}$$

has been introduced, which, on use of Mathematica [14], can be integrated to give

$$f(b) = 2 + \frac{27}{8b^2} + \frac{3}{b} + \frac{3}{2b^2}\sqrt{\frac{b}{2\pi}}\frac{(4b-9)\exp(2b)}{\mathrm{erfi}(\sqrt{2b})}, \tag{76}$$

and then, on use of (37), this can be simplified to

$$f(b) = 4 + (1-3\kappa)(4 - 9b^{-1}). \tag{77}$$

If the two models are to predict the same stress then from (74) we must have

$$n\pi w''(1)f(b) = 8(1-3\kappa)^2\Psi_{\mathrm{f}}''(1). \tag{78}$$

For the exponential model used in (23) we obtain $\Psi_{\mathrm{f}}''(1) = k_1$. If we use the exponential model in Eq. (5) we obtain $w''(1) = 4c_1$, and hence the constants c_1 and k_1 must be related by

$$n\pi c_1[4 + (1-3\kappa)(4 - 9b^{-1})] = 2k_1(1-3\kappa)^2. \tag{79}$$

In the paper [7] the exponential model with $k_1 = c_1$ was adopted for the GST and AI models in order to compare the predictions of the models for several modes of deformation for a range of values of κ. In view of the formula (37), the above relation would then give two equations relating b and κ. The only solutions of these simultaneous equations are $\kappa = 0$ and $\kappa = 1/3$, as can easily be verified, so the use of the same exponential models with the same material constants for other values of κ in [7] is inappropriate, and the resulting comparisons between the predictions of the GST and the AI models are therefore misleading. Moreover, for each different deformation considered a formula relating c_1 and k_1 different from (79) would be obtained. This means that even in the small deformation range the two models are not equivalent.

Thus, to compare the predictions of the two models, for each separate κ (or equivalently b) in uniaxial extension, for example, and for a given k_1 the formula (79) needs to be used to obtain c_1 for each b separately for the corresponding AI model. To illustrate the point the plots in Fig. 8 provide comparisons of the predictions of the two models for several values of b for both simple tension and simple shear. For this purpose it suffices to take $c_2 = k_2$ for all the considered values of b. The continuous curves correspond to the AI model and the dashed curves to the GST model. The parameter values have been set so that the continuous and dashed curves can be seen separately but by refining these parameters it is possible to arrange for the plots to be indistinguishable. It is quite clear that the predictions of the two models essentially coincide. Note that in Case A, where there is very little dispersion, $c_1 = k_1$. In Case B, where there is more dispersion, c_1 and k_1 are slightly different, while in Case C, where the dispersion is larger, close to isotropy, the values for c_1 and k_1 are quite different for both simple extension and simple shear. Note that for Case C the values of k_1 are different for simple extension and simple shear because of the role of the mean fiber direction and the different dispersions used in the two cases. We emphasize that for the plots in Fig. 8 fibers under compression were not excluded, but similar results can be obtained when compressed fibers are excluded.

4 Summary and Concluding Remarks

In contrast to the claims in the literature that compressed fibers cannot be excluded in the generalized structure tensor model, in the present paper we have shown that this is not the case by developing a rather simple and efficient method for excluding fibers under compression for the GST model. The consequences of this have been illustrated for the cases of simple tension and simple shear, and the differences between the stress responses under exclusion and non-exclusion have been highlighted. The theory presented herein can be used as a basis for a

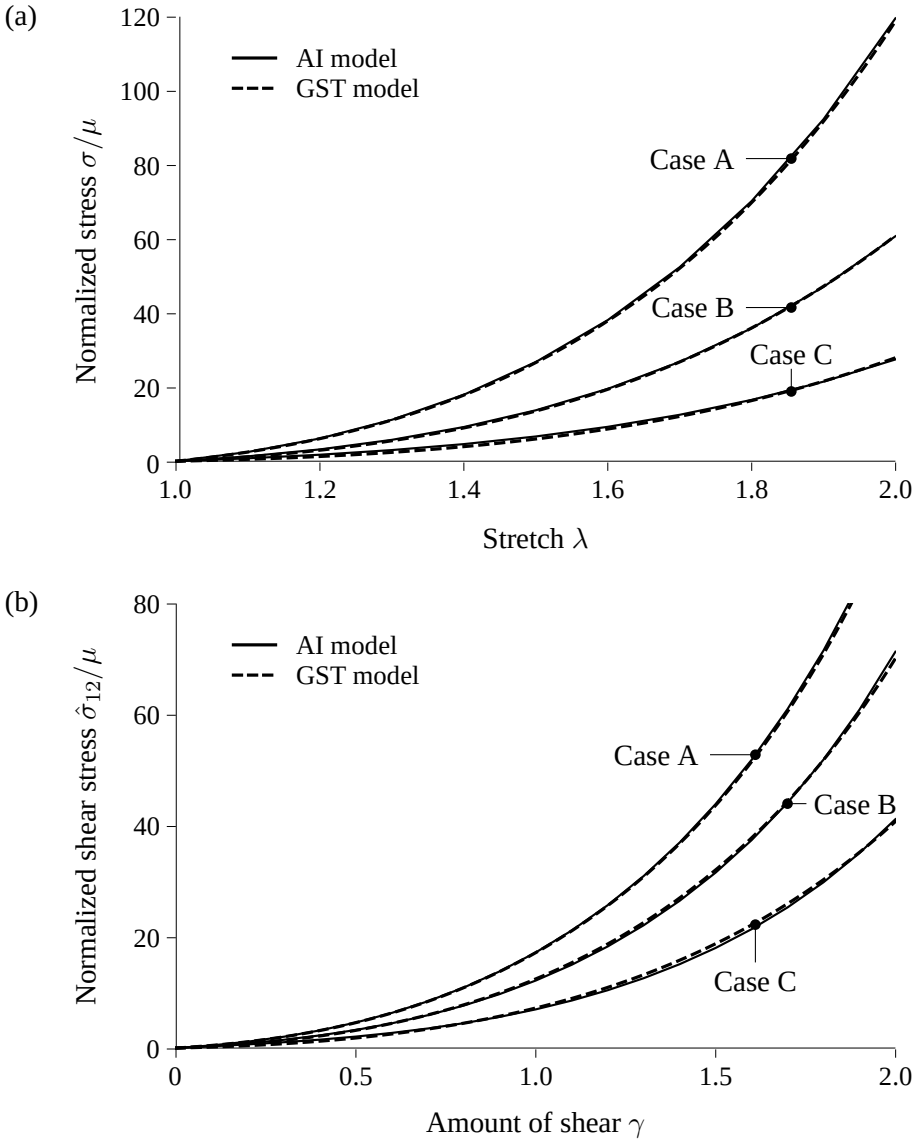

Figure 8: AI model (continuous curve) and GST model (dashed curve) for Case A (very little dispersion), Case B (intermediate dispersion) and Case C (large dispersion, close to isotropy): (a) simple tension; (b) simple shear for $\Theta_{\rm M} = 60^\circ$. Parameters are for Case A (AI: $b = 10$, $c_1 = 5$; GST: $\kappa = 0.026$, $k_1 = 5$), Case B (AI: $b = 1.5$, $c_1 = 5$; GST: $\kappa = 0.15$, $k_1 = 5.2$), Case C (AI: $b = 0.1$, $c_1 = 5$; GST for (a): $\kappa = 0.26$, $k_1 = 5.7$; GST for (b): $\kappa = 0.26$, $k_1 = 4.1$), while for all cases and the two models $c_2 = k_2 = 0.01$. Note that the factor n in (67) has been absorbed in the parameter c_1.

general implementation into a finite element program in which the dispersion parameter needs to be evaluated at each Gauss point; details of this will be provided in a subsequent paper. The present model just constitutes a small extension to the dispersion model developed in [4]. The

analysis can also be extended to the case of a non-symmetric fiber dispersion involving two dispersion parameters, as introduced in [5], and will result in two deformation dependent dispersion parameters. The GST model has also been used in considering inelastic effects such as damage in, e.g., [16] and [17]. We emphasize that we have already provided a detailed analysis of the exclusion of compressed fibers for the AI approach in [10], [11]; however, it seems that the AI approach has not been implemented in commercially available finite element programs.

In the second part of the present paper we have drawn attention to misleading statements in the literature concerning the relative values of the two approaches. Unfortunately, statements which suggest that the AI approach is superior by referring to it as the 'gold standard', are based on erroneous considerations, as we have highlighted at several locations in the preceding sections. Indeed we have shown that both models have equivalent predictive power in two examples for which the study [7] and subsequent studies have indicated significant differences which are referred to as 'errors' therein. As the above examples demonstrate, careful analysis of the literature is needed, and one should not just accept that what is published is correct.

References

[1] A. J. Schriefl, H. Wolinski, P. Regitnig, S. D. Kohlwein, and G. A. Holzapfel. An automated approach for 3D quantification of fibrillar structures in optically cleared soft biological tissues. *J. R. Soc. Interface*, 10:20120760, 2013.

[2] D. M. Pierce, W. Trobin, J. G. Raya, S. Trattnig, H. Bischof, Ch. Glaser, and G. A. Holzapfel. DT-MRI based computation of collagen fiber deformation in human articular cartilage: a feasibility study. *Ann. Biomed. Eng.*, 38:2447–2463, 2010.

[3] Y. Lanir. Constitutive equations for fibrous connective tissues. *J. Biomech.*, 16:1–12, 1983.

[4] T. C. Gasser, R. W. Ogden, and G. A. Holzapfel. Hyperelastic modelling of arterial layers with distributed collagen fibre orientations. *J. R. Soc. Interface*, 3:15–35, 2006.

[5] G. A. Holzapfel, J. A. Niestrawska, R. W. Ogden, A. J. Reinisch, and A. J. Schriefl. Modelling non-symmetric collagen fibre dispersion in arterial walls. *J. R. Soc. Interface*, 12:20150188, 2015.

[6] S. Federico and W. Herzog. Towards an analytical model of soft biological tissues. *J. Biomech.*, 41:3309–3313, 2008.

[7] D. H. Cortes, S. P. Lake, J. A. Kadlowec, L. J. Soslowsky, and D. M. Elliot. Characterizing the mechanical contribution of fiber angular distribution in connective tissue: comparison of two modeling approaches. *Biomech. Model. Mechanobiol.*, 9:651–658, 2010.

[8] A. Pandolfi and M. Vasta. Fiber distributed hyperelastic modeling of biological tissues. *Mech. Mat.*, 44:151–162, 2012.

[9] Y. Lanir and R. Namani. Reliability of structure tensors in representing soft tissues structure. *J. Mech. Behav. Biomed. Mater.*, 46:222–228, 2015.

[10] G. A. Holzapfel and R. W. Ogden. On the tension–compression switch in soft fibrous solids. *Eur. J. Mech. A/Solids*, 49:561–569, 2015.

[11] K. Li, R. W. Ogden, and G. A. Holzapfel. Computational method for excluding fibers under compression in modeling soft fibrous solids. *Eur. J. Mech. A/Solids*, 57:178–193, 2016.

[12] A. V. Melnik, H. Borja Da Rocha, and A. Goriely. On the modeling of fiber dispersion in fiber-reinforced elastic materials. *Int. J. Non-Linear Mech.*, 75:92–106, 2015.

[13] A. Gizzi, A. Pandolfi, and M. Vasta. Statistical characterization of the anisotropic strain energy in soft materials with distributed fibers. *Mech. Mat.*, 92:119–138, 2016.

[14] *Wolfram Research, Inc. Mathematica, Version 10.4.* Champaign, Illinois, 2016.

[15] R. W. Ogden. Nonlinear continuum mechanics and modelling the elasticity of soft biological tissues with a focus on artery walls. In G. A. Holzapfel and R. W. Ogden, editors, *Lecture notes from the Summer School "Biomechanics: Trends in Modeling and Simulation" in Graz, Austria, in September, 2014*, Heidelberg, 2016. Springer.

[16] H. Weisbecker, D. M. Pierce, P. Regitnig, and G. A. Holzapfel. Layer-specific damage experiments and modeling of human thoracic and abdominal aortas with non-atherosclerotic intimal thickening. *J. Mech. Behav. Biomed. Mater.*, 12:93–106, 2012.

[17] B. Fereidoonnezhad, R. Naghdabadi, and G. A. Holzapfel. Stress softening and permanent deformation in human aortas: continuum and computational modeling with application to arterial clamping. *J. Mech. Behav. Biomed. Mater.*, 61:600–616, 2016.